

von Karman Institute for Fluid Dynamics

STO-AVT-VKI Lecture Series 2016/17 – AVT 289

**Lecture Series on**

**MULTIPHYSICS PHENOMENA ANALYSIS ON  
BOUNDARY LAYER STABILITY IN  
HYPERSONIC REGIME**

September 18-20, 2017

*UNSTEADINESS IN TURBULENT SHOCK WAVE  
BOUNDARY LAYER INTERACTION*

P. Dupont  
IUSTI, Aix Marseille University, CNRS, France



# Unsteadiness in turbulent shock wave boundary layer interaction

**Pierre Dupont**

IUSTI

Aix Marseille University, CNRS UMR 7343

5 rue Enrico Fermi

Marseille, 13013

France

[pierre.dupont@univ-amu.fr](mailto:pierre.dupont@univ-amu.fr)

## **ABSTRACT**

*Shock/turbulent boundary-layer interactions produce generally unsteadiness of the shock system. This phenomenon is reviewed and analyzed, by evaluating the results of various experiments and simulations. In particular, results in the case of a shock reflection are presented. This kind of interaction is characterized by strong unsteadiness, both at low and medium frequency compared to the energetic scales of the incoming boundary layer. Some generic schemes are presented to describe the mean and unsteady fields.*

## **Contents**

<b>1.0 Introduction</b>	<b>1</b>
<b>2.0 Mean flow properties</b>	<b>2</b>
2.1 General flow organization . . . . .	2
2.2 Length of interaction . . . . .	3
2.3 Separated shear layer . . . . .	6
2.4 Relaxation region . . . . .	7
<b>3.0 Unsteadiness in the TSWBLI</b>	<b>7</b>
3.1 Shock waves unsteadiness . . . . .	7
3.2 Interaction region . . . . .	8
3.3 Spatial Links . . . . .	9
<b>4.0 Generic schemes for separated TSWBLI</b>	<b>10</b>

## **1.0 INTRODUCTION**

Shock Wave Boundary Layer Interactions (SWBLI) have been widely studied in the last decades (see for example the following review papers: [1–6]). The most commonly considered interactions concern those with

a turbulent boundary layer, although laminar or transitional interactions have also been investigated in literature. Cases under consideration covered a large range of geometric configurations (among others *normal shock interactions* ([7–9]), *blunt fin interactions* ([10, 11]), *over-expanded nozzles* ([12, 13]), *compression ramp interactions* ([14–28]) and *incident reflecting shock interactions* ([29–41]) ; the list is evidently not exhaustive). In addition, the considered flow conditions cover a large range of Mach numbers (from transonic to hypersonic values) and of Reynolds numbers (spanning at least two orders of magnitude depending on the experimental facilities).

Despite these large variations in aerodynamic and geometric parameters, several general properties have been highlighted for this family of flows. The qualitative mean organization of the flow is currently quite well understood, see [1]. Good quantitative agreement has been obtained in the particular case where the shock strength is large enough for the boundary layer to separate. In those cases, the free interaction theory proposed by [42] suggests that the separation shock properties become independent of the original cause of the separation (i.e. the flow deflection angle). Therefore, notwithstanding the difference in flow geometry, the wall pressure distributions for sufficiently separated shock reflections and compression ramps are nearly coincident (see [1]).

More recently, evidence of low frequency unsteadiness of the separation shock has been reported ([23, 24, 43, 44]). These frequencies are about two orders of magnitude below those of the energetic scales of the upstream boundary layer and their origin has been a subject of studies for two decades.

Although the precise sources of the separation shock motions are still under debate, it has been shown recently that in separated cases, the low frequency unsteadiness of the separation shock is also rather independent of the particular geometry of the flow ([27, 30, 45, 46]). For example, a dimensionless frequency of the separation shock oscillations, originally proposed for a Mach 3 compression ramp case ([23]), can be defined with a nearly constant value, whatever the particular shock induced separation that is considered (see [23, 45]). This dimensionless frequency, or Strouhal number, is defined as:

$$S_L = \frac{fL}{U_1} \quad (1)$$

where  $f$  is the characteristic shock motion frequency,  $L$  the characteristic length of the interaction (see part. 2.0) and  $U_1$  the velocity downstream the separation shock.

The document is organized as follows. In part 2.0, the mean flow properties will be detailed for the particular case of a Mach 2.3 shock reflection and a model to describe the length scale of the SWBLI will be presented. In part 3.0, details about the unsteadiness which are developing inside along the interaction will be given. Some generic scheme, derived from these results, will be presented in the part 4.0.

## 2.0 MEAN FLOW PROPERTIES

### 2.1 General flow organization

The general flow organization is detailed in the particular case of the shock reflection. The global organization of the incident shock wave boundary layer interaction was obtained by spark Schlieren visualization and PIV measurements (see figure 1(a) ), for which the flow deviation due to the incident shock is  $8^\circ$ , and the pressure gradient is strong enough for the layer to separate.

The PIV processing operate some average over the size of the interrogation window. An assessment of this space integration can be made as follows. The method implicitly assumes that for all scales, particles are convected at the local flow velocity. In inhomogeneous conditions, a problem can arise if the velocity fluctuation is affected by the finite size of the interrogation cell. A criterion was proposed by [47], who assumed that a cell

is sufficiently small if the velocity variation  $\Delta U$  over the cell is small compared to the velocity fluctuation, i.e.  $\Delta U \ll u'$ . For a cell of height  $h$ , the previous condition, after linearisation leads to:

$$h \frac{\partial U}{\partial y} \ll u' \text{ or } h \ll \frac{u'}{\partial U / \partial y} \quad (2)$$

We recognize in the right hand side member the definition of the mixing length. In the external boundary layer the mixing length is constant,  $l \simeq 0.1\delta$ . Therefore, in the external layer, it is possible to derive the simple criterion:

$$h \ll 0.1\delta \quad (3)$$

which gives an indication of an acceptable size of the interrogation window. In these experiments, the spatial resolution of the PIV measurements were of  $50\text{pixel}/\text{mm}$ , leading to a longitudinal field of view (FOV) of  $32\text{mm}$ . Since the FOV is rather reduced, and to obtain mean quantities along the whole interaction as shown in Figure 1(a), six different acquisitions, at different longitudinal positions, were necessary to obtain a final longitudinal FOV of  $160\text{mm}$ . The final effective cell size is  $0.64 \times 0.32\text{mm}^2$ , for a boundary layer thickness of  $\delta = 11\text{mm}$ . Therefore, in the incoming boundary layer, we obtain a ratio  $h/\delta = 0.06$  which satisfies the criteria defined by the relation 3. An overlap of 50 % between cells provided a final field of  $138 \times 505$  vectors, after assembly of the different acquisitions.

The maps of turbulent normal stresses (wall-normal component) is presented and superimposed on Schlieren snapshots figure 1(a). The levels of velocity fluctuations are found to increase dramatically in the interactions, and this high level persists over a long distance downstream of the interaction. The main features are highlighted in figure 1(b) as proposed in [1]. The separation region is assimilated with an isobaric region divided in two parts:

- the upstream region extends from the separation point to the reflection of the incident shock on the separated region. This region corresponds to a constant positive deviation angle.
- The downstream region is associated with a constant negative angle in order to ensure the flow reattachment. It yields the creation of an expansion wave. Pressure equilibrium between the isobaric separation and the supersonic regions is obtained by ensuring that the pressure decrease across the expansion wave is equal to its increase across the incident shock. Thus, expansion deviates the flow down to the wall at an angle approximatively equal to the imposed deviation and  $P_2 \simeq P_4$ .

Downstream from the reattachment, an equivalent reattachment shock is required to model the flow deviation necessary for achieving a wall-parallel streamline. It results in the increase in pressure found downstream from the interaction. When the interaction is fully separated, the deflection angle imposed by the first ramp becomes independent of the incident-shock intensity and consequently the pressure ratio at the separation point also becomes independent. Similar features were found for compression ramps [15], in accordance with the so-called *free interaction theory*[42].

## 2.2 Length of interaction

Shock wave boundary layer interactions (SWBLIs) present large qualitative similarities whatever the aerodynamic and geometric parameters. Nevertheless, it remains quite difficult to compare the length scales of these interactions. The characteristic length  $L$  represents the effects of the presence of the boundary layer in comparison to a purely inviscid flow. It is defined as the observed upstream shift of the shock wave  $C_S$  due to the thickening of the boundary layer, subject to the imposed pressure jump (or equivalently the angle of deviation

## Unsteadiness in turbulent shock wave boundary layer interaction

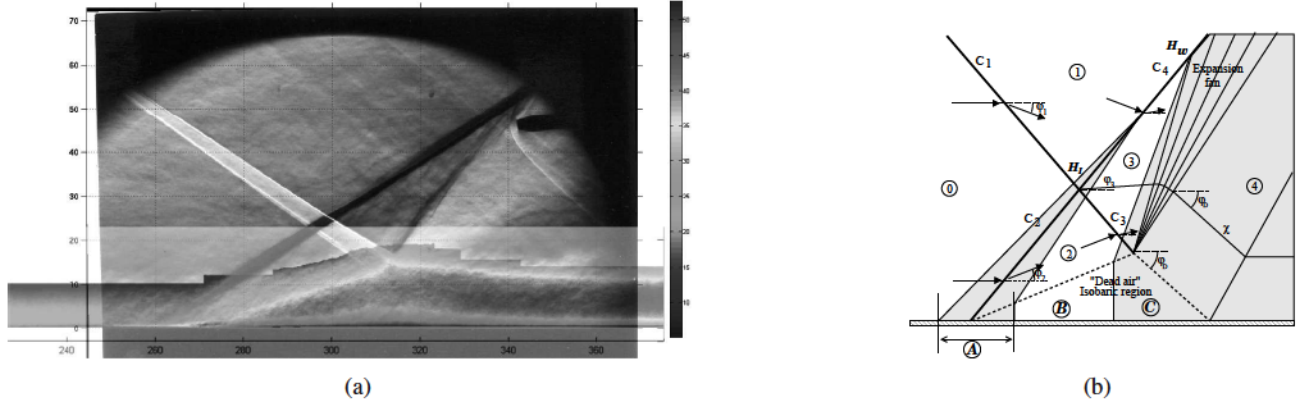


Figure 1: (a) Schlieren picture of the shock boundary layer interaction carried out in IUSTI's wind tunnel with Iso-values for rms normal velocity superimposed on the picture and (b) Inviscid equivalent scenario for shock-wave boundary layer interaction with separation[1].

of the flow). When the boundary layer is sufficiently decelerated to separate, the shock wave  $C_S$  is called the *separation shock*. For simplicity, we will keep this nomenclature for this shock wave, whatever the separation state of the flow. Hence, in the case of reflecting waves,  $L$  is defined as the distance between the foot of the separation shock and the the extrapolated wall impact point of the incident shock( see Figure 1(b) ). Similarly, in cases of for example compression corners and blunt fins,  $L$  is defined as the distance between the foot of the separation shock and the corner, respectively the obstacle. In cases with large separation,  $L$  can be considered as a rough estimate of the length of separation  $L_{sep}$  which is poorly documented in literature.

A scaling analysis was derived for the two main geometric configurations (compression corner and shock reflection) [48]. As a starting point, it is assumed that  $L$  is some function  $F_1$  of the reference flow conditions, see equation 4.

$$L = F_1(M_e, Re_\theta, \varphi, \frac{T_w}{T_{aw}}, \text{geometry}, \dots) \quad (4)$$

where  $\varphi$  is the flow deviation (the corner angle for compression ramps and the deviation angle across the incident shock in flow reflection cases).

It is now attempted to reformulate the expression in equation 4 in such a way as to obtain a relation between a non-dimensional interaction length ( $L^*$ ) and a non-dimensional interaction strength parameter that represents the tendency of the flow to separate ( $S^*$ ), in other words:

$$L^* = F_2(S^*) \quad (5)$$

where  $F_2$  is a still to be defined function. It is proposed to define the non-dimensional interaction strength parameter  $S^*$  as:

$$S^* = \frac{\Delta P}{\Delta P_{sep}} \quad (6)$$

where  $\Delta P_{sep}$  is the shock intensity needed to make the boundary layer to separate; ( $P_3 - P_1$ ) for the reflection and ( $P_2 - P_1$ ) for the compression corner, see Figure 2.

To develop this reasoning further, an inviscid model was defined based on the integral form of the conservation laws. The presence of the boundary layer is taken into account through the integral of the upstream and downstream velocity and density profiles (in other words:  $\delta^*$  and  $\theta$ ). Furthermore, it is assumed that at the exit plane,

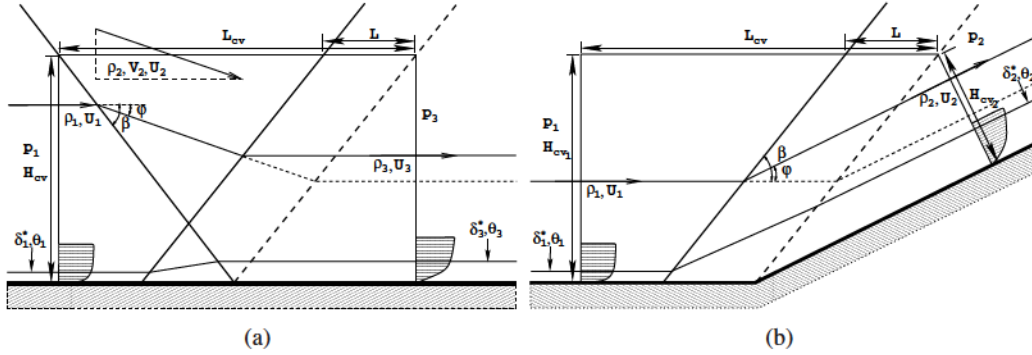


Figure 2: Control volume: (a) incident shock reflection case; (b) compression ramp case.

the pressure jump imposed by the shock system ( $\Delta P$ ) equals the inviscid value, and that the fluid is parallel to the wall. The physical cause of the interaction length may now be interpreted as a change in displacement thickness between the upstream and downstream states, creating a kind of ‘equivalent’ step at the wall.

To concretise these ideas, a control volume approach is defined, enclosing the interaction region. It is assumed that the flow is two dimensional and steady in the mean. In the formulation of the inviscid flow model, the viscous terms are inherently neglected with respect to the pressure force and the inertial terms in the deduction of the momentum conservation based formulation. The flow conditions on all sides of the control volume are prescribed by the free-stream conditions and the inviscid oblique shock relations. The presence of the boundary layer can be taken into account through the definition of the displacement thickness.

In the proposed model, the edge conditions must adhere to the inviscid shock reflection conditions. The pressure gradient imposed by the shock system will lead to a deceleration of the boundary layer and therefore to an increase of the displacement thickness through the interaction as compared with the upstream thickness. Consequently, the only way for the flow to assure mass and momentum conservation in the presence of the boundary layer is to translate the reflected shock, see figure 2(a) for the reflection case and figure 2(b) for the compression corner. This translation can be cast into an algebraic equation by considering the difference between the inviscid case (the perfect fluid solution without boundary layer and interaction) and the viscous case.

A common formulation was derived for the principal geometrical cases: the incident shock reflection and the compression ramp. The interaction length is expressed as an algebraic function of the  $M_e$ , the flow deviation  $\varphi$  and the mass flow deficit ratio between the incoming boundary layer and the outgoing boundary layer. Defining the mass flow deficit as  $\dot{m}^* = \rho U \delta^*$ :

$$\begin{aligned} L^* &= \frac{L}{\delta_{in}^*} G_3(M_e, \varphi) \\ &= \frac{\dot{m}_{out}^*}{\dot{m}_{in}^*} - 1 \end{aligned} \quad (7)$$

With:

$$G_3(M_e, \varphi) = g_3^{-1}(M_e, \varphi) = \frac{\sin(\beta) \sin(\varphi)}{\sin(\beta - \varphi)} \quad (8)$$

The new scaling for  $L$  is put to the test in figure 3 [48]. The new scaling hence appears to satisfy the desired properties concerning the separation state, while producing a curve that represents the function  $F_2$ , as defined by equation 5.

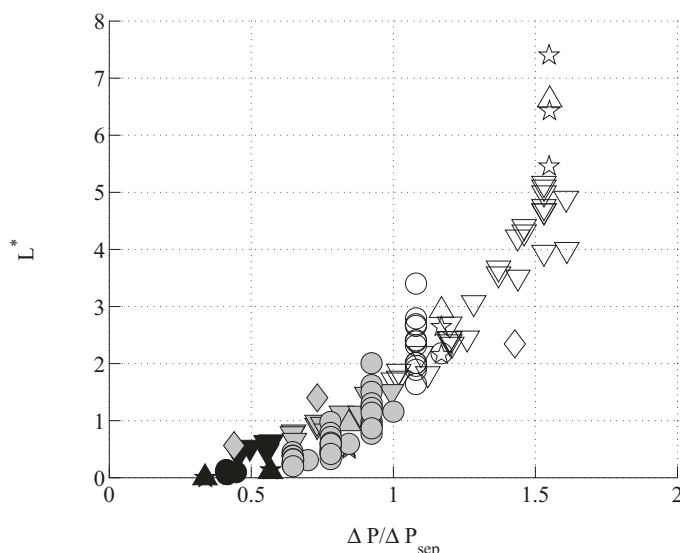


Figure 3: New scaling of the interaction length, mass balance based. Colours represent the separation state (black: attached; grey: incipient; white: separated).

### 2.3 Separated shear layer

The interaction region is now considered. Downstream from the separation point, a separated shear layer is developing. Based on the Free Interaction analysis [42] some generic properties can be expected for this region. A classical idea is to compare this region with mixing layer flows. Nevertheless, referring to canonical mixing layer raises several questions. For example, the length of development of the mixing layer is rather limited so that it is not obvious that self-similar properties can be reached. The mixing layer is embedded in a turbulent environment produced by the upstream boundary layer, and the influence of these conditions is not really known. The mixing layer makes an angle with the incoming flow, so that entrainment can be modified. Finally, the mixing layer is formed by two counter-flowing streams, which are known to produce bifurcations in the formation of large scale eddies and very probably in the related mass entrainment rate (see [49, 50]). These various aspects are now examined. First, the angle of deviation imposed to the separated shear layer at the separation is taken into account and a similarity analysis is tested in the new coordinate system. The result on the center line of the mixing layer suggests that an appropriate frame of reference (longitudinal axis along the mixing layer centerline and transverse axis perpendicular to it) should be used. The angle  $\alpha$  of the centerline of the mixing layer was derived from the position of the extrema of  $\overline{u'^2}$ . The velocity and Reynolds stresses were determined in this frame of reference. The results for the velocity fields in the mixing layer coordinate system are shown in figure 4, where  $X$  is now taken along the centerline and  $Y$  in the perpendicular direction. It turns out that, within the range of accuracy all these quantities behave in a self-similar fashion, and have shapes typical of mixing layers. Very similar results were obtained for a Mach 3 compression corner [51]. These results suggest that the separated shear layer may exhibit similar properties than canonical plane mixing layer: such considerations were used to derive simple model to describe the unsteadiness which are developing along the interaction (see part 3.0).

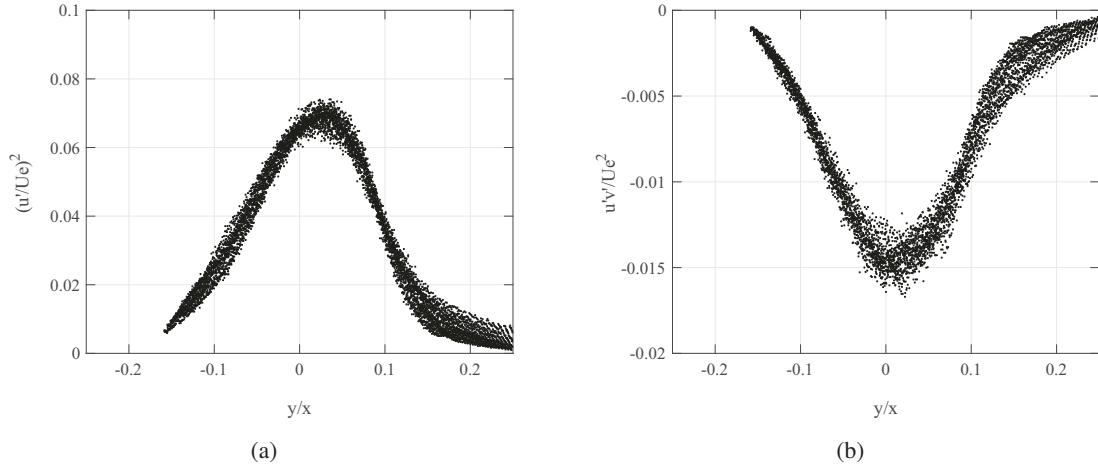


Figure 4: Velocity profiles in the mixing layer coordinate system,  $\theta = 9.5^\circ$ : (a): variance of the longitudinal velocity; (b): cross correlation normalized by  $U_c^2$ .

## 2.4 Relaxation region

Considering Figure 1(a), high level of turbulence are observed downstream from the reattachment region. Just downstream from the reattachment, the maxima of fluctuations are found far from the wall with similar level as in the separated shear layer. The relaxation of the downstream boundary layer extends over more than 10 boundary layer thickness. Nevertheless, in the near wall region, where the relaxation process is faster, new log-region can be observed scaling on the downstream wall properties. These high level of fluctuations will be related to the unsteadiness which are developing along the separated shear layer (see part. 3.0).

## 3.0 UNSTEADINESS IN THE TSWBLI

In this section, unsteady properties will be considered. Since pioneer experiments in turbulent separated SWBLI ([18, 43, 52, 53]) among others, very low frequency shock motions have been observed, whatever the particular geometry. The characteristic frequencies are about two order of magnitude lower than the energetic upstream scales of the incoming turbulent boundary layer. More recently, DNS and LES simulations confirmed these experimental results ([27, 46, 54, 55]). In the next sections the particular case of a shock reflection will be presented, similar results were observed in other geometric configurations.

### 3.1 Shock waves unsteadiness

Experimental and numerical results show that when the shock intensity is strong enough to make the boundary layer separate, the foot of the shock becomes unsteady and oscillates more or less randomly at very low frequencies compared with the characteristic temporal scales of the incoming boundary layer. This is illustrated Figure 5 where iso-values of normalized pre-multiplied Power Spectral Densities of the wall pressure fluctuations are reported along a Mach 2.3 shock reflection for an imposed flow deviation of  $8^\circ$ . Experimental results are reported Figure 5(a)[30] and LES results Figure 5(b)[54], where the interaction is defined by the dashed lines labeled  $X^* = 0$  and  $X^* = 1$  corresponding respectively to the mean position of the separation shock

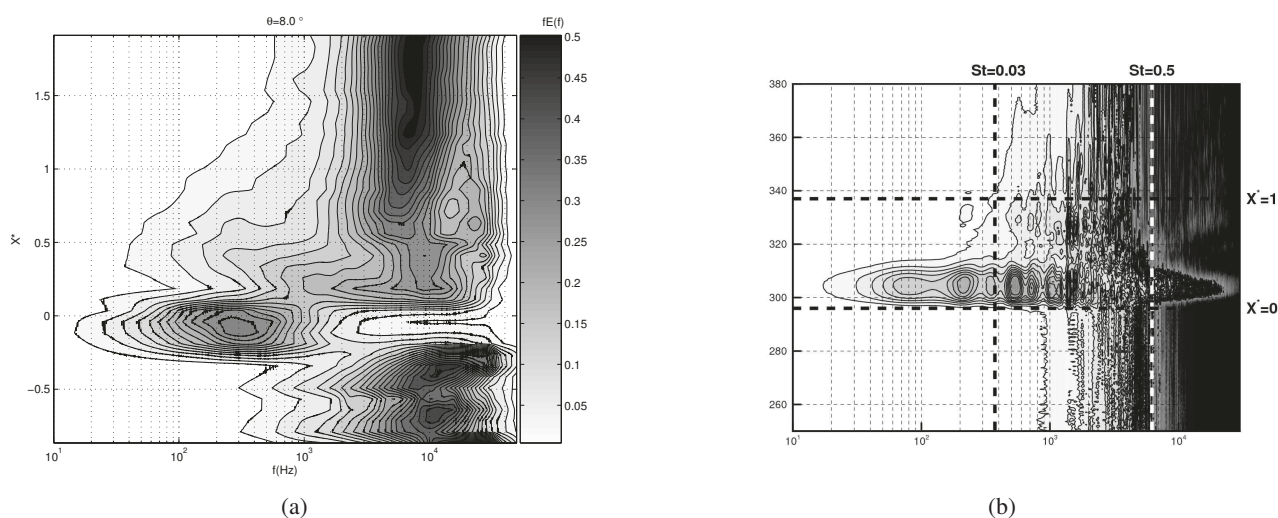


Figure 5: Pressure power spectral density along the interaction ( $\theta = 8^\circ$ ). (a) experiments and (b) LES.

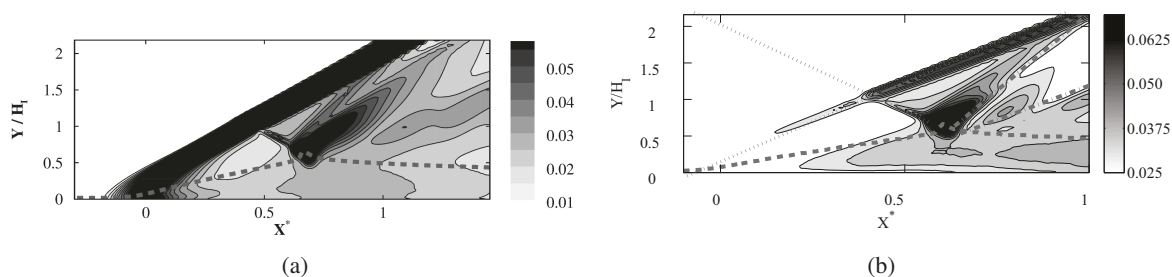


Figure 6: RMS values of the low-pass filtered ( $S_L < 0.08$ ) pressure fluctuations (a) and medium frequency with Strouhal numbers ranging from 0.3 and 0.8. (b). the dashed line denotes the sonic line.

and to the extrapolation down to the wall of the impingement shock. Very low frequencies are observed in the region of the separation ( $X^* \simeq 0$ ). As mentioned in the Introduction, a dimensionless frequency (Strouhal number) can be defined as:  $S_L = fL/U_e$ , where  $L$  is the length of interaction and  $U_e$  the external velocity. Typical values of 0.03 are observed in TSWBLI [23]. From the LES data, it is possible to derive the spatial map of the pressure fluctuations. They are reported Figure 6(a) for the low frequencies ( $S_L < 0.08$ ) and Figure 6(b) for the medium frequencies ( $0.3 < S_L < 0.8$ ). It is clear from these figures that low frequencies oscillations involve the whole separation shock. On the other hand, medium frequencies shock oscillations are observable only far from the wall.

### 3.2 Interaction region

Downstream from the separation region ( $X^* > 0.2$ ), a complex evolution of the PSD is observed (see Figures 5 and 6). Low frequencies are still present in the interaction region, but are vanishing downstream from the reattachment region. As for the external part of the separation shock, energetic medium frequencies are developing along the interaction region (see Figure 5 and 6(b)). Similar results were observed in incompressible separated

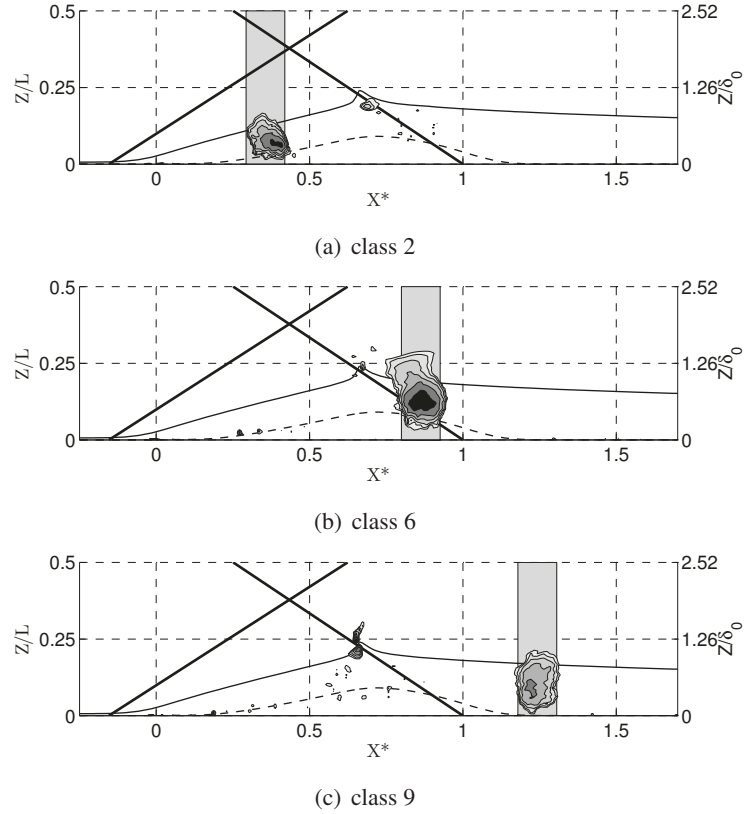


Figure 7: Vortical structures educed from the conditionally averaged data by means of the Q criterion. The shock-system location is outlined by the set of thick solid lines. The thin solid line and the dashed one indicate respectively the Mach line and the average zero mass flux lines.

flows. If the medium frequencies involved in both cases similar Strouhal numbers ( $S_L \simeq 0.5$ ) [30], large differences were observed for the low frequencies which involved Strouhal number of about 0.1 in incompressible cases and 0.03 for compressible ones [30]. Medium frequencies are generally related with some large coherent structures which are developing along the separated shear layer. As reported part 2.0, this region can be compared with a mixing layer flow. In such flows, some large coherent structures are expected to develop, but in high Reynolds turbulent flows, simple schemes of eduction are generally not efficient to identify such events. The properties of these structures have been documented thanks to experimental and numerical data. Recently, a new eduction scheme has been derived in order to evaluate their stochastic properties (spectral content, size, convection velocity, trajectory) [56]. These large coherent structures are advected and are growing along the separated shear layer, then they are shed in the downstream region (see Figure 7(c)) as suggested from the iso-values of velocity fluctuations (see Figure 1(a)).

### 3.3 Spatial Links

The results presented in the previous sections show that the interaction regions is developing a complex system of unsteadiness. Two main characteristic frequencies, referred respectively as low ( $S_L \simeq 0.03$ ) and medium frequencies ( $S_L \simeq 0.5$ ), have been identified. In high Reynolds cases, upstream perturbations have been shown to influence separation shock motions[26, 34, 57]. However these experiments are considered to be nearly

attached/incipient–separation configurations for which no reverse flow could be observed from Particle Image Velocimetry (PIV) measurements in a time–average sense. In the separated cases, it is clear that the low frequency separation shock motion are strongly correlated with the low frequency breathing of the separated region (see [33]).

It has also been known for decades from unsteady wall–pressure measurements that specific phase relationships are observed [23, 24, 30, 58]. For example, whatever the geometry (compression corner or shock reflection) and Mach number ( $1.5 < M < 5$ ), strong correlation at low frequency occurs between wall pressure fluctuations created by the shock unsteadiness and those downstream from the shock. The initial region of the interaction exhibits in–phase pressure fluctuations, while the region near the reattachment point presents anti–phase pressure signals. These two regions are separated by a zone of null correlation whose origin is not yet well established. Finally, as shown Figure 6(b), the separation shock motions are also involving medium frequencies, at least far from the wall.

#### 4.0 GENERIC SCHEMES FOR SEPARATED TSWBLI

Efforts have been put for many years to characterize the low frequency unsteadiness and several models derived from experimental data and numerical simulations were introduced in order to define their sources, see Morgan *et al.*[59].

In [33] a scenario of entrainment–discharge mechanism has been proposed, according to which the mixing layer at the edge of the dead–air zone entrains air from the separated bubble, and sheds it into the downstream layer. This produces a mass deficit in the recirculation, which, from time to time has to be re–fed by fresh air flowing backwards. This mechanism defines a characteristic time (or frequency), which was used to evaluate the frequency scale of the phenomenon, by assuming that the mass entrainment rate by the shear layer follows the same laws as a canonical mixing layer, in particular for the Mach number dependence. A normalized Strouhal number was defined:

$$S_l = \frac{fl}{U_1} = \Phi(M_c)g(r, s)\frac{l}{h} \quad (9)$$

where  $\Phi(M_c)$  is the normalized spreading rate of the compressible mixing layers,  $g(r, s)$  a parametric function of the velocity ( $r$ ) and density ( $s$ ) ratios across the separated shear layer and  $l/h$  the aspect–ratio of the separation bubble. As the mixing process is related to the dynamics of the large coherent structures developing along the separated shear layer, this relation suggest a direct influence of the geometry of the flow (its aspect ratio) and an indirect influence between the medium frequencies and the low frequency breathing of the separation bubble. The model was able to give some relevant scaling for low–frequency shock unsteadiness in various SWBLI configurations (see figure 8), but detailed descriptions of the process were not addressed. Other works propose to consider the whole interaction as a dynamic system with its own transfer function. Initially suggested in [52], this approach has been recently re–considered in the case of a Mach 2.3 shock reflection in [61], where the interaction is proposed to act as a low pass filter for the upstream perturbations. This analysis, based on the similitude properties of the flow inside the first part of the interaction, estimated with success the characteristic time scale of shock unsteadiness in the IUSTI (Institut Universitaire des Systèmes Thermiques Industriels) 8° interaction. These two models differ mainly on the nature of the low frequency unsteadiness: Toubert & Sandham’s model suggests a broad band mechanism without a particular time scale, limited by the equivalent cut–off frequency of the system. On the contrary, the model of Piponniau *et al* suggests the existence of a characteristic frequency, eventually with some time fluctuations, due to the turbulence and/or some harmonics in the entrainment time scales. Both types of unsteadiness could even cohabit, as suggested in [61]. Several attempt has been carried out in order to identify intrinsic low frequency unsteady modes in the separated

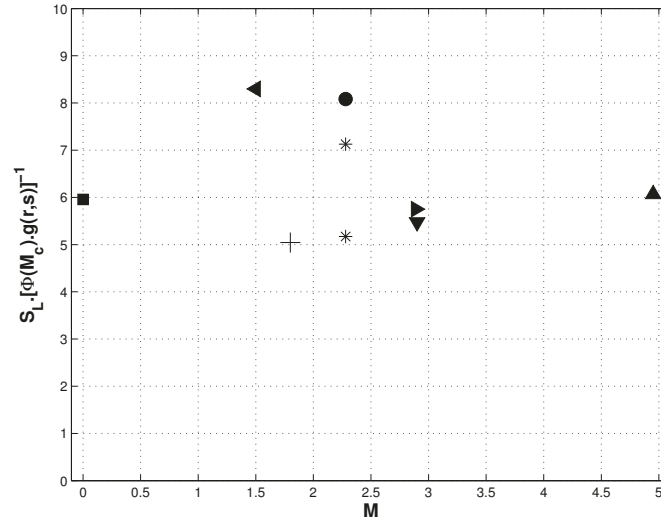


**Figure 8: Dimensionless frequency of the shock oscillation normalized as suggested by relation 9: (■) subsonic separation from [60], other symbols are TSWBLI**

region. In incompressible cases, global stability analysis suggest the development of discrete unsteady convective modes [62]. The authors suggest a non-linear mechanism between these convective modes to explain the low frequency breathing of the separation bubble: nevertheless, no precise mechanism was provided. Similar analysis was generalized for similar transonic[63–65] and supersonic cases[66]. It has been found from the global stability analyses performed on compressible flow configurations without shock ( $M < 0.75$ ) that these flows behave similarly to the incompressible separated flows. For the transonic cases, two different behaviors have been observed depending on the geometrical configuration. For the case of the flow around an airfoil with a positive angle of attack, it was confirmed that the low-frequency buffet was related to a global instability mode. For the other cases, namely a  $Me < 0.85$  flow over a bump and the  $M = 2$  shock reflection, a major conclusion from the global stability analysis is that the base flowfield is stable, regardless of the configuration. The low frequency unsteadiness are not modal in nature whatever the level of compressibility considered while. The flow responses to optimal perturbations have consequently been studied, highlighting that both the transonic and supersonic flows under consideration may act as selective noise amplifiers. Optimal perturbation analyses have demonstrated that the flow acts as selective noise amplifiers, with a high sensitivity to disturbances in the same medium frequency range that the one associated with unstable modes found for cases without shocks. Consequently it seems that, regardless of the compressibility level, the low frequency unsteadiness are not modal in nature and have to be related to: either a nonlinear mechanism involving unstable (or transiently amplified) convective modes of higher frequencies, or a selective amplification of external low-frequency perturbations.

If the precise origin of these low frequencies is still under debate, some experimental results obtained in various SWBLIs are not yet clearly explained by these different models. For example, the characteristic phase relationships and coherency (as recalled in part 3.3). From LES simulation, the details of the physical mechanism have been explored, giving rise to the upstream and downstream influence on the shock motion [54, 55]; it also identifies spatially the zones controlling the motion of the different part of the shock system, along with the

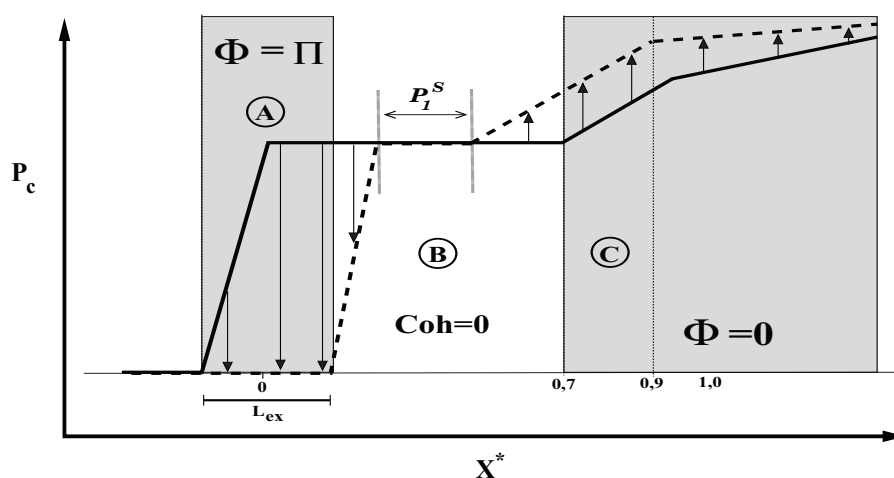


Figure 9: Descriptive model of the conditional wall–pressure for small (dashed line) and large bubbles (solid line) in the wind-tunnel frame. Grey zones denote the regions in which a constant phase  $\Phi$  between the shock location and the pressure can be derived from the model. Arrows denote the pressure variations when moving from the large to the small bubble.

frequency ranges which are involved.

A descriptive model from conditional analysis of the low frequency wall pressure was derived from LES [55]. When the pressure is conditioned vs the size of the separation bubble, it is found to increase (respectively to decrease) when the bubble is decreasing (respectively increasing). Conditional wall pressures for small and large separation bubble, respectively downstream and upstream separation shock motions, are reported in figure 9 and induced phase relationships between the separation–shock location and wall–pressure variations are reported, when defined, in the grey regions. This simple sketch, derived for a shock reflection, makes it possible to describe the main features of low frequency wall–pressure fluctuations identified in separated turbulent SWBLI, namely:

- the anti–phase relationship in region *A*, with large intermittent pressure fluctuations relating to the pressure step across the separation shock.
- the in–phase relationship in region *C* and downstream, as long as the adverse gradient pressure does not vanish, with a maximum of the coherent pressure fluctuations centered in region *C*.
- a buffer zone, corresponding to the isobaric region region *B* (see Figure 1(b)) where in-phase, anti-phase or null coherent pressure fluctuations can be obtained. In our case, the isobaric region for small bubbles is vanishing and the extent of the region bounded by black vertical lines in figure 9 is nearly reduced to a point. Therefore, in region *B*, we observe mainly equi-probable switches from in-phase to anti–phase, and vice versa. This is the reason why no correlation between the wall pressure and the shock motions is obtained in this region. Moreover, in the downstream part of this region, coherent pressure fluctuations should increase from nearly null fluctuations to values of the same order as those in region *C*.

The conditional streamwise pressure profiles have been analyzed in the supersonic region of the interaction by using the same approach as that described for wall pressure. A new inviscid equivalent scheme of the shock-wave/boundary-layer interaction has been derived: it is basically an extension of the classical scheme proposed by Delery and Marvin[1], sketched in figure 1(b). Nevertheless, the whole separated region cannot be

associated with an isobaric region since only region  $B$  exhibits a pressure gradient close to zero. In the second part of the separated region (subregion  $C$ ), a significant adverse pressure gradient develops and is associated with large unsteady pressures. Moreover, it has been found from LES data analysis[55] that the shock system balances the pressure between the subsonic and supersonic regions by means of reflected compression waves produced by the reflection of the incident shock through the boundary layer[67]. Such compression waves, seen in figure 1(a) as dark lines located upstream from the expansion fan, are inconsistent with the single ramp scenario described in figure 1(b).

A new conceptual model, sketched in figure 10, is introduced to alleviate these shortcomings. A new second ramp is added just upstream from the impingement point of the incident-shock. It splits the equivalent subsonic region into two parts which can be associated respectively with regions  $B$  and  $C$  of the scheme introduced in figure 9. The first ramp results in a flow deflection compatible with the *free interaction theory*, *i.e.* independent of the size of the separation. The flow then undergoes a second deviation, due to the second ramp, and imposes an increase in pressure. In the inviscid supersonic region, this leads to the creation of the shock  $C'_3$  which intersects the separation shock  $C_4$  near  $H_w$ , thus strengthening the separation shock up to the value  $C'_4$ .

The low-frequency unsteadiness of the first ramp can be associated with the bubble breathing, which is linked to the extent of region  $B$  with a small or null pressure gradient (isobaric region in cases of large separated bubbles). This is the origin of the longitudinal displacements of the separation shock. On the other hand, the second ramp unsteadiness involves a specific region of the interaction, typically  $0.6 < X^* < 0.9$ , see figure 9. This corresponds to region  $C$ , where large pressure gradients are observed, downstream from the nearly isobaric region, as in subsonic separated cases. This pressure gradient ensures the connection with downstream pressure in the separated region and generates weak pressure fluctuations at low frequency.

The influence of medium-frequency coherent structures on the reflection of incident shock have been shown figure 6(b). Average values induced by the convection of coherent structures along the mixing layer are found in region  $B$  while the foot of the incident shock/reflected compression waves experiences much higher values. Large values are also recovered along the path of compression waves up to the location  $H_w$  at which they intercept the separation shock, in agreement with the characteristics-based analysis of the propagation of pressure disturbances, as developed in Agostini *et al.*[54]. Therefore, the inviscid equivalent model sketched in figure 10 can be extended to the medium-frequency unsteadiness. It is achieved by linking the medium-frequency unsteadiness to the second ramp in order to include the pressure variations due to the interaction of the convective structures with the adverse pressure gradient of region  $C$ . Therefore, the second ramp, associated with region  $C$  in the scheme of figure 9, displays oscillations at two different characteristic frequencies:

- low frequency with  $S_L \simeq 0.03$ , associated with the bubble breathing,
- a medium frequency with  $S_L \simeq 0.5$ , associated with the convective structures and the rapid decrease in their time scale in this region.

It should be stressed that the scheme presented does not explain the origin of low-frequency unsteadiness and their possible correlation with medium frequencies generated by the coherent convective structures developing in the separated shear layer. Nonetheless, whatever the precise mechanism linking the two frequency ranges, the proposed simple inviscid scheme will describe accurately the whole field of unsteady pressure within and downstream from the interaction. In particular, the phase relationships, the coherence maps, the evolution of the pressure standard deviation and the convective velocities obtained along the head shock for various separation state are qualitatively reproduced.

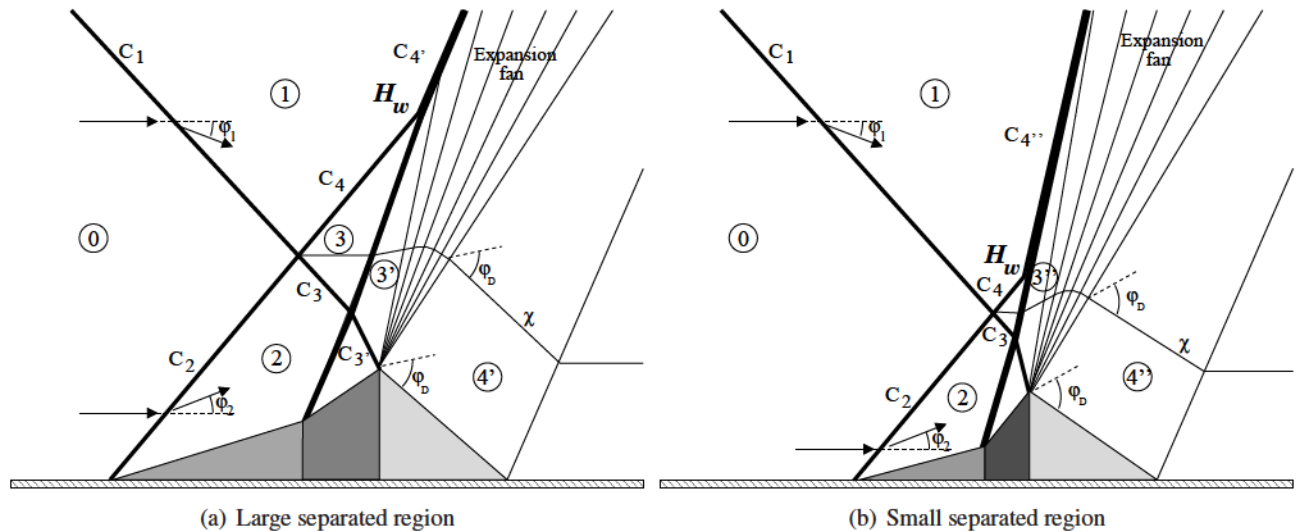


Figure 10: Inviscid equivalent scenario of the shock wave boundary layer interaction depending on the interaction length.

## ACKNOWLEDGMENTS

This work was partly supported by the Agence National de la Recherche (ANR) through the DECOMOS project from the Blanc program and from the CNES through the research program ATAC as well as from the Labex Mécanique Et Complexité. The research team was granted access to high-performance computing resources of Institut du Développement et des Ressources en Informatique Scientifique (IDRIS) under allocations 2009-021877 and 2010-021877 made by Grand Equipement National de Calcul Intensif (GENCI). These supports are gratefully acknowledged.

## REFERENCES

- [1] Déleroy, J. M. and Marvin, J. G., "Shock wave - boundary layer interactions," Tech. rep., 1986.
- [2] Viswanath, P. R., "Shock-wave-turbulent-boundary-layer interaction and its control: A survey of recent developments," *Sādhanā*, Vol. 12, 1988, pp. 45–104.
- [3] Dolling, D. S., "Fifty years of shock-wave/boundary-layer interaction research: what next," *AIAA Journal*, Vol. 39, No. 8, August 2001, pp. 1517–1531.
- [4] Smits, A. J. and Dussauge, J. P., *Turbulent shear layers in supersonic flow*, AIP Press, 2nd ed., 2006.
- [5] Clemens, N. T. and Narayanaswamy, V., "Shock/Turbulent Boundary Layer Interactions: Review of Recent Work on Sources of Unsteadiness," *39th Fluid Dynamics Conference and Exhibit, San Antonio, Texas, USA, AIAA-2009-3710*, 22-25 June 2009.
- [6] Déleroy, J. M. and Dussauge, J. P., "Some physical aspects of shock wave/boundary layer interactions," *Shock Waves*, Vol. 19, No. 6, December 2009, pp. 453–468.
- [7] Atkin, C. J. and Squire, L. C., "A study of the interaction of a normal shock wave with a turbulent boundary layer at Mach numbers between 1.30 and 1.55," *European J. Mechanics*, Vol. 11, No. 1, 1992, pp. 93–118.

- [8] Bruce, P. J. K. and Babinsky, H., “Unsteady shock wave dynamics,” *Journal of Fluid Mechanics*, Vol. 603, 2008, pp. 463–473.
- [9] Bur, R., Benay, R., Galli, A., and Berthouze, P., “Experimental and numerical study of forced shock-wave oscillations in a transonic channel,” *Aerospace Science and Technology*, Vol. 10, 2008, pp. 265–278.
- [10] Brusniak, L. and Dolling, D. S., “Physics of unsteady blunt-fin-induced shock wave/turbulent boundary layer interactions,” *Journal of Fluid Mechanics*, Vol. 273, 1994, pp. 375–409.
- [11] Ünalms, Ö. H. and Dolling, D. S., “On the possible relationship between low frequency unsteadiness of shock-induced separated flow and Goertler vortices,” *27th AIAA Fluid Dynamics Conference, New Orleans, Louisiana, USA, AIAA-1996-2002*, 17-20 June 1996.
- [12] Frey, M. and Hagemann, G., “Status of flow separation prediction in rocket nozzles,” *AIAA Paper*, , No. 98-3619, 1998.
- [13] Bourgoing, A. and Reijasse, P. H., “Experimental analysis of unsteady separated flows in a supersonic planar nozzle,” *Shock Waves*, Vol. 14, No. 4, 2005, pp. 251–258.
- [14] Thomke, G. J. and Roshko, A., “Incipient separation of a turbulent boundary layer at high Reynolds number in two-dimensional supersonic flow over a compression corner,” Tech. Rep. DAC-59819, NASA Ames Research Center, January 1969.
- [15] Spaid, F. W. and Frishett, J. C., “Incipient separation of a supersonic, turbulent boundary layer, including effect of heat transfer,” *AIAA Journal*, Vol. 10, No. 7, July 1972, pp. 915–922.
- [16] Settles, G. S., Fitzpatrick, T. J., and Bogdonoff, S. M., “Detailed study of attached and separated compression corner flowfields in high Reynolds number supersonic flow,” *AIAA Journal*, Vol. 17, 1979, pp. 579–585.
- [17] Ardouneau, P. L., “The Structure of Turbulence in a Supersonic Shock-Wave/Boundary-Layer Interaction,” *AIAA Journal*, Vol. 22, No. 9, 1984, pp. 1254–1262.
- [18] Dolling, D. S. and Or, C. T., “Unsteadiness of the shock wave structure in attached and separated compression ramp flows,” *Experiments in Fluids*, Vol. 3, 1985, pp. 24–32.
- [19] Smits, A. J. and Muck, K. C., “Experimental study of three shock wave / turbulent boundary layer interactions,” *Journal of Fluid Mechanics*, Vol. 182, 1987, pp. 291–314.
- [20] Kuntz, D. W., Amatucci, V. A., and Addy, A. L., “Turbulent Boundary-Layer Properties Downstream of the Shock-Wave / Boundary-Layer Interaction,” *AIAA Journal*, Vol. 25, No. 5, May 1987, pp. 668–675.
- [21] Selig, M. S., Andreopoulos, J., Muck, K. C., Dussauge, J. P., and Smits, A. J., “Details of a shock - separated turbulent boundary layer at a compression corner,” *AIAA Journal*, Vol. 27, No. 7, July 1989, pp. 862–869.
- [22] Erenkil, M. E. and Dolling, D. S., “Correlation of Separation Shock Motion with Pressure Fluctuations in the Incoming Boundary Layer,” *AIAA Journal*, Vol. 29, No. 11, November 1991, pp. 1868–1877.
- [23] Erenkil, M. E. and Dolling, D. S., “Unsteady wave structure near separation in a Mach 5 compression ramp interaction,” *AIAA Journal*, Vol. 29, No. 5, May 1991, pp. 728–735.

- [24] Thomas, F. O., Putman, C. M., and Chu, H. C., “On the mechanism of unsteady shock oscillation in shock wave/turbulent boundary layer interaction,” *Experiments in Fluids*, Vol. 18, 1994, pp. 69–81.
- [25] Beresh, S. J., Clemens, N. T., and S.Dolling, D., “Relationship between upstream turbulent boundary layer velocity fluctuations and separation shock unsteadiness,” *AIAA Journal*, Vol. 40, No. 12, dec 2002, pp. 2412–2422.
- [26] Ganapathisubramani, B., Clemens, N. T., and Dolling, D. S., “Effects of upstream boundary layer on the unsteadiness of shock–induced separation,” *Journal of Fluid Mechanics*, Vol. 585, 2007, pp. 369–394.
- [27] Wu, M. and Martin, M. P., “Analysis of shock motion in shockwave and turbulent boundary layer interaction using direct numerical simulation data,” *Journal of Fluid Mechanics*, Vol. 594, January 2008, pp. 71–83.
- [28] Ringuette, M., Wu, M., and Martin, M. P., “Low Reynolds Number effects in a Mach 3 Shock/Turbulent–Boundary–Layer Interaction,” *AIAA Journal*, Vol. 46, No. 7, July 2008, pp. 1884–1887.
- [29] Green, J., “Reflexion of an oblique shock wave by a turbulent boundary layer,” *Journal of Fluid Mechanics*, Vol. 40, 1970, pp. 81–95.
- [30] Dupont, P., Haddad, C., and Debiève, J. F., “Space and time organization in a shock induced boundary layer,” *Journal of Fluid Mechanics*, Vol. 559, 2006, pp. 255–277.
- [31] Pirozzoli, S. and Grasso, F., “Direct numerical simulation of impinging shock wave / turbulent boundary layer interaction at  $M=2.25$ ,” *Physics of Fluid*, Vol. 18, 2006.
- [32] Toubert, E. and Sandham, N. D., “Oblique shock impinging on a turbulent boundary layer: low-frequency mechanisms,” *38th AIAA Fluid Dynamics Conference, Seattle, Washington, USA, 23-26 June 2008*.
- [33] Pionniau, S., Dussauge, J. P., Debiève, J. F., and Dupont, P., “A simple model for low-frequency unsteadiness in shock-induced separation,” *Journal of Fluid Mechanics*, Vol. 629, 2009, pp. 87–108.
- [34] Humble, R. A., Elsinga, G. E., Scarano, F., and Van Oudheusden, B. W., “Three-dimensional instantaneous structure of a shock wave/turbulent boundary layer interaction,” *Journal of Fluid Mechanics*, Vol. 622, 2009, pp. 33–62.
- [35] Souverein, L. J., Van Oudheusden, B. W., Scarano, F., and Dupont, P., “Application of a dual-plane particle image velocimetry (dual-PIV) technique for the unsteadiness characterization of a shock wave turbulent boundary layer interaction,” *Measurement Science and Technology*, Vol. 20, No. 7, July 2009, pp. 074003 (16pp).
- [36] Garnier, E., “Stimulated Detached Eddy Simulation of three–dimensional shock / boundary layer interaction,” *Shock Waves*, Vol. 19, No. 6, December 2009, pp. 479–486.
- [37] Toubert, E. and Sandham, N. D., “Comparison of three large–eddy simulations of shock–induced turbulent separation bubbles,” *Shock Waves*, Vol. 19, No. 6, December 2009, pp. 469–478.
- [38] Pirozzoli, S., Beer, A., Bernardini, M., and Grasso, F., “Computational analysis of impinging shock–wave boundary layer interaction under conditions of incipient separation,” *Shock Waves*, Vol. 19, No. 6, December 2009, pp. 487–497.

- [39] Souverein, L. J., Dupont, P., Debiève, J. F., Dussauge, J. P., Van Oudheusden, B. W., and Scarano, F., “Effect of Interaction Strength on Shock Wave Boundary Layer Interaction: Unsteady Behavior,” *AIAA Journal*, Vol. 48, No. 7, 2010, pp. 1480–1493.
- [40] Souverein, L., *On the scaling and unsteadiness of shock induced separation*, Phd thesis, Delft University of Technology and the Université de Provence - Aix-Marseille I, March 2010.
- [41] Priebe, S., Tu, J. H., Rowley, C. W., and Martín, M. P., “Low-frequency dynamics in a shock-induced separated flow,” *Journal of Fluid Mechanics*, Vol. 807, 2016, pp. 441–477.
- [42] Chapman, D. R., Kuehn, D. M., and Larson, H. K., “Investigation of separated flow in supersonic and subsonic streams with emphasis of the effect of transition,” Tech. rep., 1957.
- [43] Dolling, D. S. and Murphy, M. T., “Unsteadiness of the separation shock wave structure in a supersonic compression ramp flowfield,” *AIAA Journal*, Vol. 21, No. 12, dec 1983, pp. 1628–1634.
- [44] Dolling, D. S. and Brusniak, L., “Separation shock motion in fin, cylinder, and compression ramp-induced turbulent interactions,” *AIAA Journal*, Vol. 27, No. 6, jun 1989, pp. 734–742.
- [45] Dussauge, J. P., Dupont, P., and Debiève, J. F., “Unsteadiness in shock wave boundary layer interactions with separation,” *Aerospace Science and Technology*, Vol. 10, 2006, pp. 85–91.
- [46] Toubert, E. and Sandham, N. D., “Large-eddy simulation of low-frequency unsteadiness in a turbulent shock-induced separation bubble,” *Theoretical and Computational Fluid Dynamics*, Vol. 23, No. 2, 2009, pp. 79–107.
- [47] J.P., D. and P. D., “On critical aerodynamic phenomena in compressible turbulent flows and their measurement: an issue for PIV and optical methods,” *Keynote Lectures, Pivnet II, Delft 6-8 juin*, 2005.
- [48] Souverein, L., Bakker, P., and Dupont, P., “A scaling analysis for turbulent shock wave boundary layer interactions,” *Journal of Fluid Mechanics*, Vol. 714, 2013, pp. 505–535.
- [49] Forliti, D., Tang, B., and Strykowski, P., “An experimental investigation of planar countercurrent turbulent shear layers,” *J. Fluid Mech.*, Vol. 530, 2005, pp. 241–264.
- [50] Strykowski, P. J., Krothapalli, A., and Jendoubi, S., “The effect of counterflow on the development of compressible shear layers,” *Journal of Fluid Mechanics*, Vol. 308, 1996, pp. 63–96.
- [51] Helm, C., Martin, M., and Dupont, P., “Characterization of the shear layer in a Mach 3 shock / turbulent boundary layer interaction,” *Journal of Physics: Conference Series*, Vol. 506, 2014.
- [52] Plotkin, K., “Shock wave oscillation driven by turbulent boundary layer fluctuations,” *AIAA Journal*, Vol. 13, No. 8, 1975, pp. 1036–1040.
- [53] Andreopoulos, J. and Muck, K. C., “Some new aspects of the shock wave - boundary layer interaction in compression ramp flows,” *Journal of Fluid Mechanics*, Vol. 180, 1987, pp. 405–428.
- [54] Agostini, L., Larchevêque, L., Dupont, P., Debiève, J., and Dussauge, J., “Zones of influence and shock motion in a shock boundary layer interaction,” *AIAA Journal*, Vol. 50, No. -6, june 2012, pp. 1377–1387.

- [55] Agostini, L., Larchevêque, L., and Dupont, P., “Mechanism of shock unsteadiness in separated shock/boundary-layer interactions,” *Physics of Fluids*, Vol. 27, No. 12, 2015, pp. 126103.
- [56] Jiang, T., Larchevêque, L., and Dupont, P., “Eduction scheme for convective structures in turbulent compressible separated flow,” *8th International Symposium On Turbulence and Shear Phenomena (TSFP8), Poitiers ( FRANCE ), August 2013.*
- [57] Humble, R. A., Scarano, F., and Van Oudheusden, B. W., “Unsteady Effects in an Incident Shock Wave/Turbulent Boundary Layer Interaction,” *Journal of Fluid Mechanics*, Vol. 635, 2009, pp. 47–74.
- [58] Debiève, J. F. and Dupont, P., “Dependence between shock and separation bubble in a shock wave / boundary layer interaction,” *Schock Waves*, Vol. 19, No. 6, 2009, pp. 499–506.
- [59] Morgan, B., Duraisamy, K., Nguyen, N., Kawai, S., and Lele, S. K., “Flow physics and RANS modelling of oblique shock/turbulent boundary layer interaction,” *Journal of Fluid Mechanics*, Vol. 729, 2013, pp. 231–284.
- [60] Kiya, M. and Sasaki, K., “Structure of a turbulent separation bubble,” *Journal of Fluid Mechanics*, Vol. 137, 1983, pp. 83–113.
- [61] Toubert, E. and Sandham, N., “Low-order stochastic modelling of low-frequency motions in reflected shock-wave/boundary-layer interactions,” *Journal of Fluid Mechanics*, Vol. 671, No. 3, 2011, pp. 417–465.
- [62] Ehrenstein, U. and Gallaire, F., “Two-dimensional global low-frequency oscillations in a separating boundary-layer flow,” *Journal of Fluid Mechanics*, Vol. 614, 2008, pp. 315–327.
- [63] Merle, M., *Approches numériques pour l’analyse de stabilité globale d’écoulements pariétaux en régime subsonique*, Ph.D. thesis, ENSAM, 2015.
- [64] Merle, M., Ehrenstein, U., and Robinet, J.-C., “Global stability of compressible laminar flow over a bump: an absorbing boundary conditions approach,” *10th EUROMECH Fluid Mechanics Conference, Copenhagen, Denmark, September 14-18, 2014.*
- [65] Sartor, F., Mettot, C., Bur, R., and Sipp, D., “Unsteadiness in transonic shock-wave/boundary-layer interactions: experimental investigation and global stability analysis,” *Journal of Fluid Mechanics*, Vol. 781, 10 2015, pp. 550–577.
- [66] Guiho, F., Alizard, F., and Robinet, J.-C., “Instabilities in oblique shock wave/laminar boundary-layer interactions,” *Journal of Fluid Mechanics*, Vol. 789, 2016, pp. 1–35.
- [67] Henderson, L. F., “The reflexion of a shock wave at a rigid wall in the presence of a boundary layer,” *Journal of Fluid Mechanics*, Vol. 30, No. 04, 1967, pp. 699.